Acoustic Attenuation in Self-Affine Porous Structures

Steven R. Pride*
Lawrence Berkeley National Laboratory, 1 Cyclotron Road MS 90-1116, Berkeley, California 94720, USA

Yder J. Masson†
University of California at Berkeley, Department of Earth and Planetary Sciences, 307 McCone Hall, Berkeley, California 94720-4767, USA

(Received 31 August 2006; published 30 October 2006)

As acoustic waves propagate through fluid-filled porous materials possessing heterogeneity in the elastic compressibility at scales less than wavelengths, the local wave-induced fluid-pressure response will also possess spatial heterogeneity that correlates with the compressibility structure. Such induced fluid-pressure gradients equilibrate via fluid-pressure diffusion causing wave energy to attenuate. This process is numerically simulated using finite-difference modeling. It is shown here, both numerically and analytically, that in the special case where the compressibility structure is a self-affine fractal characterized by a Hurst exponent H, the wave's quality factor Q (where Q^{-1} is a measure of acoustic attenuation) is a power law in the wave's frequency ω given by $Q \propto \omega^{H}$ when $|H| \ll 1$, and given by $Q \propto \omega^{\tanh H}$ in general.

DOI: 10.1103/PhysRevLett.97.184301 PACS numbers: 43.20.+g, 81.05.Rm, 83.60.Bc, 83.60.Uv

Understanding the physics of mechanical wave propagation in porous materials impacts a wide range of applications ranging from the exploration of Earth's crust, to the design of sound-absorbing materials, to the nondestructive evaluation of fractured materials. From a fundamental physics perspective, perhaps the greatest challenge is to understand the way that heterogeneity across all length scales smaller than the acoustic wavelength affects the nature of the wave propagation.

In order to define porous-material properties, one needs to consider samples that contain a minimum of roughly 3 grains to the side. Most natural porous materials such as rocks and sediments in the earth have heterogeneity in the porous-continuum properties (e.g., the elastic moduli, density, and fluid-flow permeability of the grain packs) at nearly all scales greater than a few grain sizes ($\geq 10^{-3}$ m). Sound-absorbing porous materials can be manufactured to have heterogeneity over these scales as well. Seismic wavelengths used for exploration of the Earth's crust are typically in the range from 1 to 100 m. Further, airborne sound, upon entering sound-absorbing porous materials, typically has wavelengths on the order of 0.1 to 1 m. There are thus a wide range of so-called "mesoscopic" length scales l that are larger than grain sizes d (i.e., can be modeled as a porous continuum), but smaller than acoustic wavelengths λ. Figure 1 graphically depicts the length-scale relation $\lambda > l > d$. For the purpose of modeling an acoustic experiment, it is generally necessary to define the porous-continuum properties at a scale (resolution) of roughly a tenth of a wavelength.

Many studies [1–10] have focused on the effective acoustic properties of fluid-filled porous media in the presence of mesoscopic length-scale heterogeneity. When an acoustic wave compresses a sample of porous material containing mesoscopic heterogeneity, the fluid-pressure response will be relatively large in regions where the compressibility of the framework of grains is large, and small where the framework compressibility is small. A process of fluid-pressure equilibration (i.e., viscous fluid

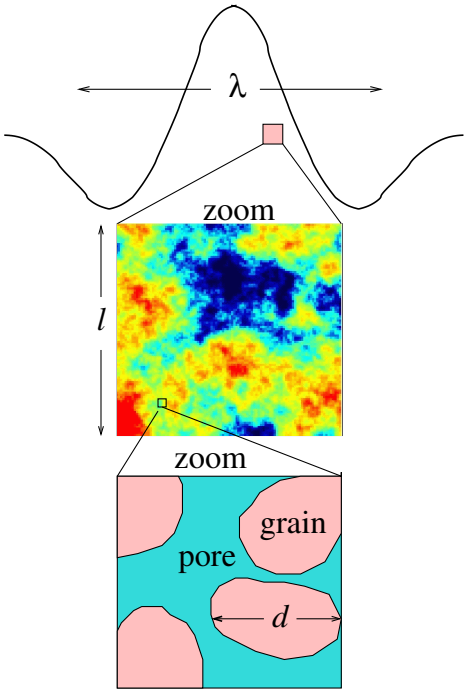

FIG. 1 (color online). Depiction of the length-scale relation $\lambda > l > d$, where λ is the wavelength of the acoustic pulse, l is the linear dimension of a sample containing mesoscopic-scale heterogeneity in the local porous-continuum properties, and d is a characteristic size of a grain.

flow) ensues that is capable of attenuating significant amounts of acoustic wave energy.

In the present Letter, we focus on the complex bulk modulus $K_u(\omega)$ of sealed samples of porous media that contain a self-affine fractal structure in the local compressibility of the framework of grains. The subscript u denotes "undrained" which signifies that no fluid exchanges into or out of the sample are allowed to occur. An undrained modulus is of interest because it can be shown (e.g., Ref. [11]) that over the acoustic frequencies ω used in both exploration work and audible-sound absorption ($1\ \mathrm{Hz} < \omega/2\pi < 10\ \mathrm{kHz}$), no significant fluid exchanges occur between the averaging volumes used to define the effective properties and the surrounding material. Any induced flow that needs to be allowed for is occurring within the averaging volume (sample) and is due to the presence of mesoscopic-scale heterogeneity.

To obtain the complex undrained bulk modulus, one can first apply a temporal step in the normal stress $-P$ that acts uniformly on the sealed exterior faces of a sample of material. The induced volumetric strain of the sample $\epsilon = \delta V/V$ is then measured through time, and a temporal Fourier transform taken of both the applied stress and measured deformation to yield $K_u(\omega) = -\tilde{P}(\omega)/\tilde{\epsilon}(\omega)$. The compressional attenuation associated with the phase shift between stress and strain is conveniently described using a quality factor Q_{Ku} defined as

$$\frac{4\pi}{Q_{Ku}} = \frac{\text{total energy lost per stress period}}{\text{average energy reversibly stored per period}} \tag{1}$$

$$= \frac{\mathrm{Im}\{K_u(\omega)\}}{\mathrm{Re}\{K_u(\omega)\}}. \tag{2}$$

It is straightforward to demonstrate that the physical definition of Eq. (1) is equivalent to the operational definition of Eq. (2) [12].

Our approach here is to measure $K_u(\omega)$ numerically by performing finite-difference simulations of the above experiment. Details of how the finite-difference algorithm works are given by Masson and Pride [13,14]. The numerical simulations are based on the laws of poroelasticity [15,16] that provide a continuum description allowing for fluid-pressure changes and fluid flow in addition to the elastic deformation and acceleration of the material. The region Ω occupied by a sample under study is discretized into a Cartesian grid at a scale Δx that still implicitly contains within it enough grains ($\Delta x > 3d$) to justify a porous-continuum description of the local physics. The local porous-material properties (elastic moduli of the framework of grains, permeability, density) are distributed over the pixels (2D) or voxels (3D) of size Δx, and the complex bulk modulus of the sample determined by numerically performing the experiment of the previous paragraph.

Let C be an elastic modulus associated with the framework of grains that is specified at each grid point within the sample and that fluctuates locally over the grid. The fluctuations $\Delta C(a\Delta x)$ in C associated with each length scale $a\Delta x$, where $a > 1$, generally vary in real materials as the scale factor a varies. A self-affine fractal means that

$$\Delta C(a\Delta x) \propto a^H \Delta C(\Delta x), \tag{3}$$

where H is called the Hurst exponent ($H = 1$ corresponds to a self-similar fractal). In practice, since Δx is a finite length ($> 3d$), the fluctuation $\Delta C(\Delta x)$ at the smallest scale $a = 1$ is taken to be the standard of deviation of the probability distribution used to randomly populate the grid with C values.

We generate self-affine fractal structure within our synthetic samples using the following algorithm: (1) Generate a pseudorandom realization $W(\mathbf{x})$ of the white noise associated with the desired statistical distribution of the material property over the grid points $\mathbf{x}$; (2) calculate a spatial Fourier transform $\tilde{W}(\mathbf{k})$ of this white noise; (3) multiply the white noise with the spectral filter $\tilde{F}(\mathbf{k}) \propto |\mathbf{k}|^{-E/2-H}$ representing the correlation function of the self-affine fractal where E is the Euclidean-space dimension; (4) calculate the inverse Fourier transform of the filtered white noise; and (5) normalize to the desired variance and add the appropriate mean to obtain the final realization of the self-affine fractal material property. It has been numerically verified that self-affine structure generated in this manner possesses the scaling of Eq. (3) in both 2D and 3D.

The compressional attenuation as a function of frequency $Q_{Ku}^{-1}(\omega)$ numerically determined for a material possessing self-affine structure in the bulk modulus of the dry framework of grains is shown in Fig. 2. A Gaussian distribution was used to generate a single realization of the random fractal structure. At low frequencies, there is observed a power-law relation $Q_{Ku}^{-1}(\omega) \propto \omega$ that can be attributed to the finite size of the sample (as will be explained shortly). At high enough frequencies where the fluid-pressure-diffusion penetration length $\delta = \sqrt{D/\omega}$ (D is the fluid-pressure diffusivity) is much smaller than the size of the sample, the finite-size of the sample does not influence the diffusion process and a more interesting power-law relation is observed $Q_{Ku}^{-1}(\omega) \propto \omega^{-H}$. The example given in Fig. 2 is a 2D simulation (implicitly, a 3D experiment in which no deformation occurs in the third dimension which necessitates the shear modulus to be measured in order to obtain K_u [14]); however, the same scaling holds for a fully 3D experiment.

Figure 3 gives the high-frequency power-law exponent of $Q_{Ku}^{-1}(\omega)$ corresponding to materials covering a range of H values. When the Hurst exponent has a large magnitude compared to one ($|H| \gg 1$), the attenuation exponent tends to either $+1$ (large negative H) or -1 (large positive H). This suggests the following scaling relation valid for all H

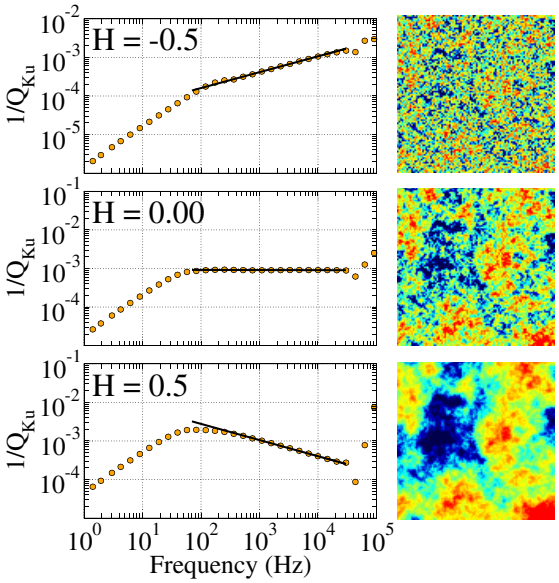

FIG. 2 (color online). Results of 2D numerical simulations of $Q_{Ku}^{-1}(\omega)$ for synthetic samples that have different Hurst exponents. The symbols are numerical data and the solid line corresponds to ω^{-H}. To the right are images of the self-affine structure present in the porous-continuum elastic modulus.

$$Q_{Ku}^{-1}(\omega) \propto \omega^{-\tanh H} \tag{4}$$

that, in Fig. 3, is seen to do an adequate job of fitting the numerical data. Equation (4) and Figs. 2 and 3 are the main results of this Letter.

We now explain these observations. The rate at which energy is locally being lost per unit volume of porous material is $(k/\eta)|\nabla p_f|^2$, where k is the local fluid-flow permeability, η is the fluid viscosity, and p_f the fluid pressure. If, as in the above examples, the amount of dissipated energy in each cycle is small compared to the

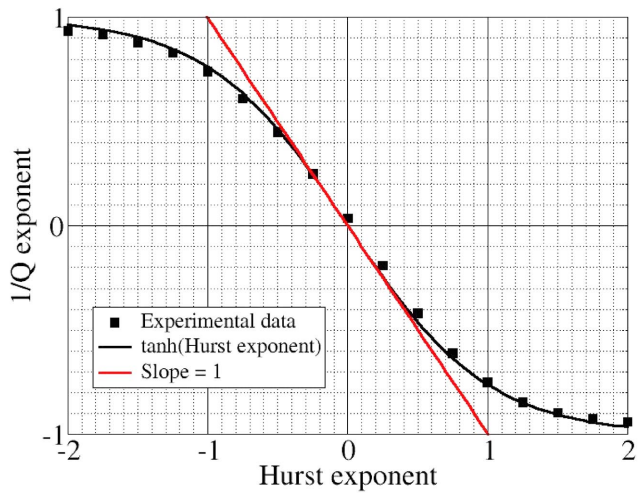

FIG. 3 (color online). Demonstration that $Q_{Ku}^{-1}(\omega) \propto \omega^{-\tanh H}$ does a fine job fitting the numerical data.

amount of stored energy, the average energy reversibly stored per unit volume is half the peak stored energy $K_U\epsilon^2$, where K_U is the local (and real) undrained bulk modulus and ϵ the local volumetric strain. Equation (1) then gives

$$Q_{Ku}^{-1} = \frac{1}{\omega\eta}\frac{\int_\Omega k|\nabla p_f|^2 dV}{\int_\Omega K_U\epsilon^2 dV}. \tag{5}$$

An approximate analysis of this expression is provided that retains the essential elements required to produce the attenuation scaling law of Eq. (4).

Each length scale $a\Delta x$ will make its own contribution to Q_{Ku}^{-1}. If the only heterogeneity in the system occurred at the length scale $a\Delta x$, the attenuation curve $Q_a^{-1}(\omega)$ associated exclusively with this scale a would rise linearly in ω up to a peak value, then descend as $\omega^{-1/2}$ [6–10]. Peak attenuation at scale a occurs at the frequency ω_a at which the fluid pressure just has time to diffuse across the distance $a\Delta x$ in a single cycle; i.e., it occurs at the frequency $\omega_a = D/(a\Delta x)^2$. Here, D is the fluid-pressure diffusivity that is well approximated as (cf. Ref. [11]) $D = kK_f/(\eta\phi)$ where K_f is the fluid's bulk modulus and ϕ is porosity.

We will make the approximation that the full attenuation curve $Q_{Ku}^{-1}(\omega)$ in the presence of all length scales corresponds to the envelope bounding the sum of the attenuation curves coming from each length scale. In the presence of a continuum of length scales a, this is very well approximated as $Q_{Ku}^{-1}(\omega) = Q_a^{-1}(\omega_a)\ \forall\ a$.

To determine the peak values $Q_a^{-1}(\omega_a)$ of the attenuation associated with each scale a, we return to Eq. (5). The local pressure gradient driving the fluid flow is created by the volumetric compression acting on the heterogeneous grain pack and is approximated as $|\nabla p_f| \approx \Delta C(a\Delta x)\epsilon/a\Delta x$, where C is the elastic modulus responsible for creating a fluid-pressure change in the grain pack from the applied volumetric strain; i.e., $C = -p_f/\epsilon$ and is, like K_U, defined assuming undrained (sealed sample) conditions. Expressions that detail how C depends on the bulk modulus of the dry framework of grains and on the moduli of the fluid and solid phases can be found in many places including Ref. [11]. Further, in this "order-of-magnitude" analysis, we replace all locally varying fields by their mean values in the system (denoted with $\langle\rangle$) to obtain an estimate of the peak attenuation associated with scale a

$$Q_a^{-1}(\omega_a) \approx \frac{\langle k\rangle[\Delta C(a\Delta x)]^2}{\omega_a\eta(a\Delta x)^2\langle K_U\rangle} = \frac{\langle\phi\rangle[\Delta C(a\Delta x)]^2}{K_f\langle K_U\rangle}, \tag{6}$$

where

$$\omega_a = \frac{\langle k\rangle K_f}{\eta\langle\phi\rangle(a\Delta x)^2} \tag{7}$$

was used for the frequency of peak attenuation at scale a. Equation (6) predicts that the peak attenuation associated

with a given scale is proportional to the square of the fluctuation at that scale.

To obtain the full curve for the self-affine material, we employ the definition of a self-affine fractal $\Delta C(a\Delta x) = a^H \Delta C(\Delta x)$ and rearrange Eq. (7) to give an expression for a in terms of ω_a. Putting this in Eq. (6) gives the desired frequency scaling law

$$Q_a^{-1}(\omega_a) = Q_{Ku}^{-1}(\omega) = \frac{\langle\phi\rangle[\Delta C(\Delta x)]^2}{K_f\langle K_U\rangle}\left(\frac{\omega}{\omega_1}\right)^{-H}, \quad (8)$$

where ω_1 is the ω_a of Eq. (7) evaluated at $a = 1$. The result of Eq. (8) also demonstrates that the attenuation curve is proportional to the variance $[\Delta C(\Delta x)]^2$ of the probability distribution used to randomly distribute the elastic moduli through the sample; a result that has also been numerically confirmed.

In the limits that $|H| \to \infty$, two other scaling rules emerge. As $H \to -\infty$, the only fluctuations present in the sample are those occurring at the smallest scale $a = 1$. Across the finite bandwidth we study, this means we are always in the low-frequency regime where attenuation is increasing linearly with frequency. To explain this linear scaling in ω, we again appeal to Eq. (5). At low enough frequencies, the diffusive penetration of the fluid pressure across the low-diffusivity patches of size Δx (the only patches of significance when $H \to -\infty$) occurs rapidly during each stress period, and any remaining pressure gradients are decreasing linearly with decreasing ω not because the diffusion distance is changing, but because the average fluid-pressure difference Δp_f between two local patches is decreasing with ω. Using theoretical results from Ref. [7], one has in this case that $|\nabla p_f| \approx \Delta p_f(\omega)/\Delta x = \alpha(\eta\Delta x\epsilon/k)\omega$, where α is a dimensionless material property bounded as $0 < \alpha < 1$ (cf. Ref. [7] for the detailed nature of α). Using this in Eq. (5) gives that $\lim_{H\to-\infty} Q_{Ku}^{-1} \propto \omega$ as is numerically observed in the simulations.

As $H \to +\infty$, the dominant fluctuation is that at the scale $a = s$ of the sample itself. In this scenario, over the finite frequency bandwidth available, we are always in the high-frequency regime where fluid-pressure penetration distances are less than the scale $s\Delta x$ of the sample. The sample-scale fluctuation of the elastic moduli is thus responsible for a sample-scale fluctuation of the fluid pressure so that the fluid-pressure gradient to be used in Eq. (5) is independent of frequency and given by $|\nabla p_f| \approx \Delta C(s\Delta x)\epsilon/(s\Delta x)$. Using this in Eq. (5) predicts that $\lim_{H\to+\infty} Q_{Ku}^{-1} \propto \omega^{-1}$ as is numerically observed. Combining these results for both the large and small $|H|$ limits yields $Q_{Ku}^{-1} \propto \omega^{-\tanh H}$, which is consistent with the numerical data.

The fact that there exists a simple relation between the frequency exponent for the acoustic attenuation in a self-affine porous material and the Hurst exponent of the structure is the central "interesting" result of this Letter. Many earth scientists (e.g., [17–19]) believe that a reasonable stochastic model for earth materials is self-affine structure in the physical properties with $-1/2 < H < 0$ (property fluctuations decreasing with increasing scale). We encourage laboratory (or field) experimentalists to look for the power-law relation $Q_{Ku}^{-1} \propto \omega^{-H}$ that might hold in such heterogeneous earth materials. Unfortunately, this requires performing acoustic (or quasielastostatic) measurements on samples much larger than normally considered. To obtain two decades of length-scale variation within a sample, one needs to work with sample sizes on the order of tens of centimeters to a meter. Most laboratory protocols for measuring attenuation employ samples that are several centimeters in size.

The work of S. R. P. was performed under the auspices of the U.S. Department of Energy and supported specifically by both the Geosciences Research Program of the DOE Office of Basic Energy Sciences, Division of Chemical Sciences, Geosciences and Biosciences and by the Fossil Energy Program administered by NETL (Contract No. CO2O5CH11231).

*Electronic address: srpride@lbl.gov
†Electronic address: yder_masson@berkeley.edu

[1] J. E. White, N. G. Mikhaylova, and F. M. Lyakhovitsky, Izv., Acad. Sci., USSR, Phys. Solid Earth (Engl. Transl.) **11**, 654 (1975).
[2] J. E. White, Geophysics **40**, 224 (1975).
[3] A. N. Norris, J. Acoust. Soc. Am. **94**, 359 (1993).
[4] B. Gurevich and S. L. Lopatnikov, Geophys. J. Int. **121**, 933 (1995).
[5] S. Gelinsky and S. A. Shapiro, Geophys. J. Int. **128**, F1 (1997).
[6] S. R. Pride and J. G. Berryman, Phys. Rev. E **68**, 036603 (2003).
[7] S. R. Pride and J. G. Berryman, Phys. Rev. E **68**, 036604 (2003).
[8] S. R. Pride, J. G. Berryman, and J. M. Harris, J. Geophys. Res. **109**, B01 201 (2004).
[9] D. L. Johnson, J. Acoust. Soc. Am. **110**, 682 (2001).
[10] Y. Tserkovnyak and D. L. Johnson, J. Acoust. Soc. Am. **114**, 2596 (2003).
[11] S. R. Pride, in *Hydrogeophysics*, edited by Y. Rubin and S. Hubbard (Springer, The Netherlands, 2005), p. 253.
[12] R. J. O'Connell and B. Budiansky, Geophys. Res. Lett. **5**, 5 (1978).
[13] Y. J. Masson, S. R. Pride, and K. T. Nihei, J. Geophys. Res. **111**, B10 305 (2006).
[14] Y. J. Masson and S. R. Pride, J. Geophys. Res. (to be published).
[15] M. A. Biot, J. Acoust. Soc. Am. **28**, 168 (1956).
[16] M. A. Biot, J. Appl. Phys. **33**, 1482 (1962).
[17] L. Klimes, Pure Appl. Geophys. **159**, 1811 (2002).
[18] M. Pilkington and J. Todoeschuck, Geophys. J. Int. **102**, 205 (1990).
[19] S. M. Flatté and R. Wu, J. Geophys. Res. B **93**, 6601 (1988).